DISCRETE AND CONTINUOUS
DYNAMICAL SYSTEMS–SERIES B
Volume **00**, Number **0**, Xxxx **XXXX**

Website: http://AIMsciences.org

pp. **000–000**

CYLINDRICAL SHELL BUCKLING: A CHARACTERIZATION OF LOCALIZATION AND PERIODICITY

Abstract. A hypothesis for the prediction of the circumferential wavenumber of buckling of the thin axially-compressed cylindrical shell is presented, based on the addition of a length effect to the classical (Koiter circle) critical load result. Checks against physical and numerical experiments, both by direct comparison of wavenumbers and via a scaling law, provide strong evidence that the hypothesis is correct.

G.W. Hunt

Centre for Nonlinear Mechanics
University of Bath
Bath BA2 7AY, UK

G.J. Lord

Department of Mathematics
Heriot-Watt University
UK

M.A. Peletier

Centrum voor Wiskunde en Informatica
PO Box 94079
1090 GB Amsterdam, NL

1. **Introduction.** For an important class of long structures, applied in-plane compression is relieved by buckling on a local wavelength ℓ that is small in comparison with the overall length L. Two distinctive types of response, distributed and localized, have been found in such circumstances. Some buckle patterns, like that formed by the long thin compressed plate supported around its perimeter, distribute themselves along the full length of the structure; depending on the boundary conditions the induced pattern may be periodic or near-periodic, but the tendency is to spread or share out the imposed end-shortening. Others are predominately localized, the structure finding it easier to accommodate the shortening by concentrating it to some portion of the available length. The difference is fundamental, and it is our primary purpose here to illustrate this difference by direct reference to the buckling of a thin cylindrical shell under axial compression.

The most important criterion for determining the form of response is found at the critical *bifurcation* point, where the buckle pattern first emerges as a linear eigenvalue problem. If this is of the *stable-symmetric* or *supercritical* form, the buckle pattern which emerges is likely to be periodic or distributed. If on the other hand it is *unstable-symmetric* or *subcritical*, the pattern is likely to emerge as periodic but then rapidly localize as the deflection grows. Examples of both forms

Key words and phrases. Shell buckling, post-buckling, bifurcation, localization, von Kármán–Donnell equations.

of behaviour are many, and are often summarised by reference to the compressed elastic strut on a nonlinear elastic foundation. (See Wadee [17] for a recent review of subcritical responses, and Everall and Hunt [9] for supercritical behaviour.)

But certain problems do not fall neatly into either of these two categories. The buckle pattern of the long, unpressurized, axially-compressed, cylindrical shell is a hybrid, localized with respect to the length but periodic around the circumference [13]. This offers a unique perspective on the instability process in general, and in particular on the contrasting mechanisms of localization and periodicity. Mode locking and mode jumping, for example, which are strong features of periodic behaviour [9], have no role in localization. This leads to the observation that, whereas the circumferential wavenumber appears to be fixed at the *pre*-buckling stage of the loading and remains so until far into the post-buckling range, localization only appears at an early stage of the *post*-buckling. However, it does takes effect rapidly and is effectively complete at load levels commensurate with the actual buckling load of the system.

Based on these observations, we hypothesise that the classical linear eigenvalue view, as seen in well-known Koiter circle [12], can be reinterpreted to predict the circumferential wavenumber of initial buckling. From a combination of reference to well-known experiments [1, 19, 8], modern implicit time-stepping dynamic finite element analyses [15], and our own numerical solutions of the von Kármán–Donnell equations employing a Galerkin circumferential reduction, we find evidence to support this hypothesis. This comes from two complementary directions. First, direct experimental evidence of the circumferential wave number offers straightfoward comparisons. Secondly, when coupled with the wavelength prediction, the minimum load reached in the numerical Galerkin scheme is found to scale as $(t/R)^\alpha$, where t is the shell thickness, R is the radius, and α is about 1.3. This compares well with the variation of failure load in a five different sets of experiments, which span the range $1.30 < \alpha < 1.49$. It has been noted by Calladine [5] and others that the scaling of the failure load differs significantly from the value of $\alpha = 1$ predicted by linearized theory, and this lends further weight to the argument that the initial buckling is governed more by the position of the classically defined *Maxwell load* [11, 4] than that obtained from the linear eigenvalue result.

The numerics suggest that a large number of possible equilibria coexist at the post-buckling load levels of interest, resulting in part from the large number of coincident eigenvalues at the Koiter circle load; the resulting tangle of equilibrium paths is much reduced in complexity by the identification of the circumferential wavenumber.

2. **Linear eigenvalue (Koiter circle) result.** For a thin elastic cylindrical shell of radius R, thickness t, and Young's Modulus E, the linearized buckling equations lead to the critical stress [12],

$$\sigma_{\text{crit}} = \frac{E}{\sqrt{3\,(1-\nu^2)}}\left(\frac{t}{R}\right) \tag{1}$$

with a mode shape that is sinosoidal both axially and circumferentially. Note that there is no apparent dependency on the length L. The locus of possible waveforms that can arise at this stress can be expressed as a semi-circle in "wavenumber space", given by,

$$(m - m_{\text{crown}})^2 + n^2 = m_{\text{crown}}^2$$

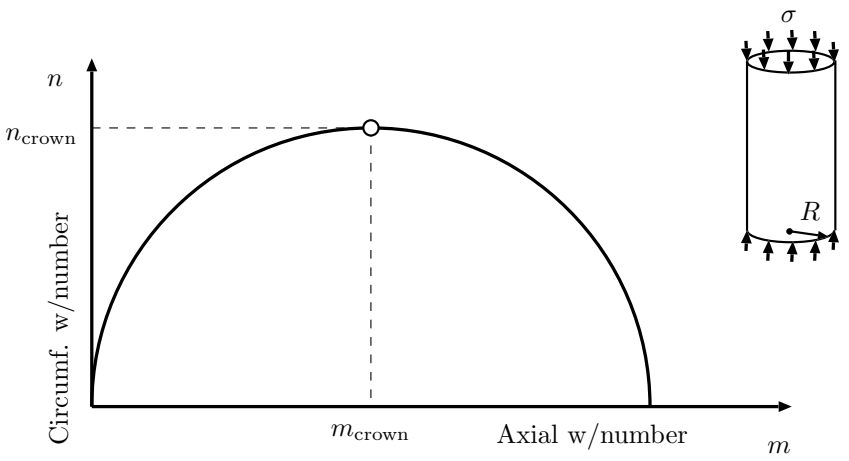

FIGURE 1. The Koiter circle

and shown in Fig.1, where the axial wavenumber $m \leq 2m_{\text{crown}}$ can take any real value for an infinitely long cylinder, while the circumferential wavenumber $n \leq n_{\text{crown}}$ must be an integer. The crown represents square waves where,

$$n_{\text{crown}} = m_{\text{crown}} = \left[\left(\frac{3}{4}\right)\left(1-\nu^2\right)\right]^{\frac{1}{4}}\sqrt{\frac{R}{t}}$$

so m refers to the number of whole axial waves in a cylinder of length $2\pi R$. Cylinders of different lengths therefore need rescaling to determine their appropriate axial wavenumber, as described below.

The classical view is that all waves on the Koiter circle are possible, and it singularly fails to distinguish that which might occur in practice. Experiments, however, show a clear preference for a single circumferential wavenumber that appears to be length-dependent [19]. Extending the argument of Croll & Yamada [18], we propose the following mechanism for wavenumber selection:

- For relatively short shells, the critical buckling mode is that which occurs on the Koiter circle with a single half wave over the length L of the cylinder. This is the suggestion made by Croll & Yamada (1999).
- For longer shells, the mode likewise occurs on the Koiter circle, but comprises two half waves over the length.
- For even longer shells, the mode may theoretically span three or more half waves over the length L; however, the available experimental data does not appear to contain shells that are sufficiently long for this to occur.

As the localization imposes a rapid change in axial wavelength, we would not expect these modes to bear any relation to the final deflected shape. However, it is known from experiments that short shells end up in a single tier [8] or symmetric [19] form of buckling, while those that are slightly longer finish in a two-tier, asymmetric, or *cross-symmetric* [13] form. If M represents the number of axial half-waves at the point of buckling in the shell of length L, we further propose that, on completion of buckling, $M = 1$ will have led to the single tier, and $M = 2$ to the two-tier, form. Rescaling to a length of $2\pi R$ as described above then gives $m = M\pi R/L$, and substituting into the Koiter circle equation leads to the following prediction of

circumferential wavenumber,

$$n^2 = M\pi\sqrt[4]{12(1-\nu^2)}\frac{R}{L}\sqrt{\frac{R}{t}} - M^2\pi^2\left(\frac{R}{L}\right)^2. \tag{2}$$

We next see how this compares with both physical and numerical experiments.

3. **Direct evidence.**

3.1. **Physical experiments.** Many experiments on axially-compressed cylindrical shells are reported in the literature, but few give enough details of the deflected shapes to enable direct comparison with equation (2). Of particular interest is the early contribution of Arbocz & Babcock [1], who mapped surfaces with a non-contact probe, and removed the shape of the initial imperfections to give accurate representations of both the pre and the post-buckled deflections. Tests were conducted on copper shells for which $R = 4$ in., $L = 8$ in., and $t = 0.004$ in. For an assumed value of Poisson's ratio $\nu = 0.3$, equation (2) gives $n = 9.37$ for $M = 1$ and $n = 13.07$ for $M = 2$; the latter agrees well with the experiments.

A typical set of results from Arbocz & Babcock [1] is given in Fig.2. At zero load, the imperfection shape is dominated by an $n = 2$ ovalization. However, this is clearly bears no relation to the triggering instability, as seen in the middle plot taken just before buckling with the initial imperfections removed. Long axial waves with a high circumferential wavenumber of $n = 13$ are now observed, having amplified components of the imperfections that are not seen at the scale of the mapping at zero load. This is plotted at a load level of 0.637 of the classical Koiter circle load (1), yet the thickness bars shown at the right indicate that the amplitude of this triggering mode is much smaller than that of the initial ovalization. In the post-buckling range shown at the bottom the amplitude is again large, and the same circumferential wavenumber of $n = 13$ is found, although the response has localized axially into the two-tier (asymmetric) form of the diamond post-buckling pattern. These results support the thesis that the circumferential wavenumber n is determined at the pre-buckling stage by the Koiter circle result, and remains fixed until advanced post-buckling. Axial buckling on the other hand is strongly influenced by the localization, and soon bears no relation to points on the Koiter circle. Arbocz & Babcock [1] also performed a Fourier breakdown of the pre-buckled shape, and found strongly developing components of both the one half wave mode at $n = 9$ and the two half waves mode at $n = 13$.

The experiments of Yamaki [19] on elastic shells made of Mylar are also of interest. A typical set of load/end-shortening curves is given in Fig.3(a). Here the elasticity of the material allows deflection far into the post-buckling range, and a continuous sequence of mode jumps to lower circumferential wavenumbers is observed. Yamaki tested cylinders of radius $R = 100$ mm and thickness $t = 0.247$ mm, ranging in length from $L = 22.7$ mm to 160.9 mm. The full set of comparisons of the initial mode of instability with equation (2) are given in Table 1. Note that the symmetric (single tier) form of buckling denoted by S occurs naturally only for the shorter cylinders; longer cylinders first buckle into the asymmetric (two-tier) form, A, but can also be persuaded into S. When it exists, the highest wavenumbers for each form is therefore included.

Experiments by Eßlinger and co-workers, again on Mylar cylinders, are similarly documented with both mode (S or A) and wavenumber, and are also suitable for comparison with equation (2). For one test highlighted by Eßlinger & Geier [8],

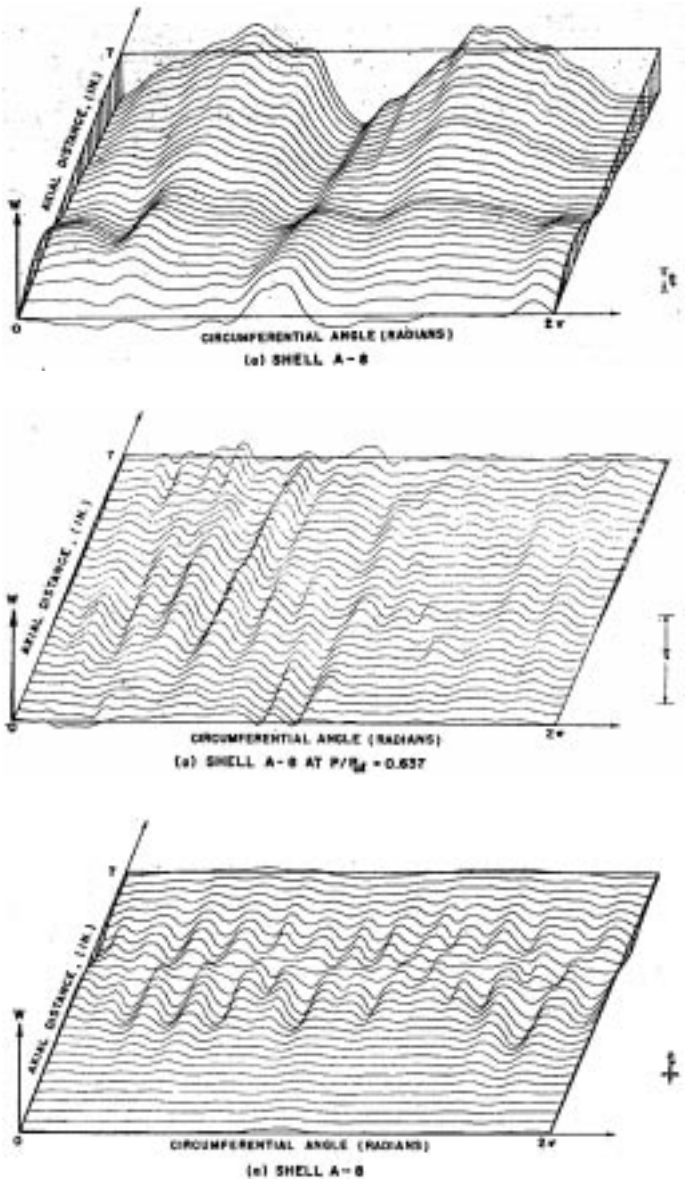

FIGURE 2. Top: imperfection shape at zero load. Middle: Deflections just before buckling with initial imperfections removed. Bottom: Post-buckled shape. Note that the bars at the right indicate the scale of deflection relative to thickness t. (After Arbocz & Babcock [1].)

$t = 0.190$ mm, $R = 100$ mm, $L = 100$ mm, and the asymmetric form of buckling occurs at $n = 15$; this compares well with the prediction of $n = 14.9$ from equation (2). A second series of tests is given in Table 2. Again comparison is good except

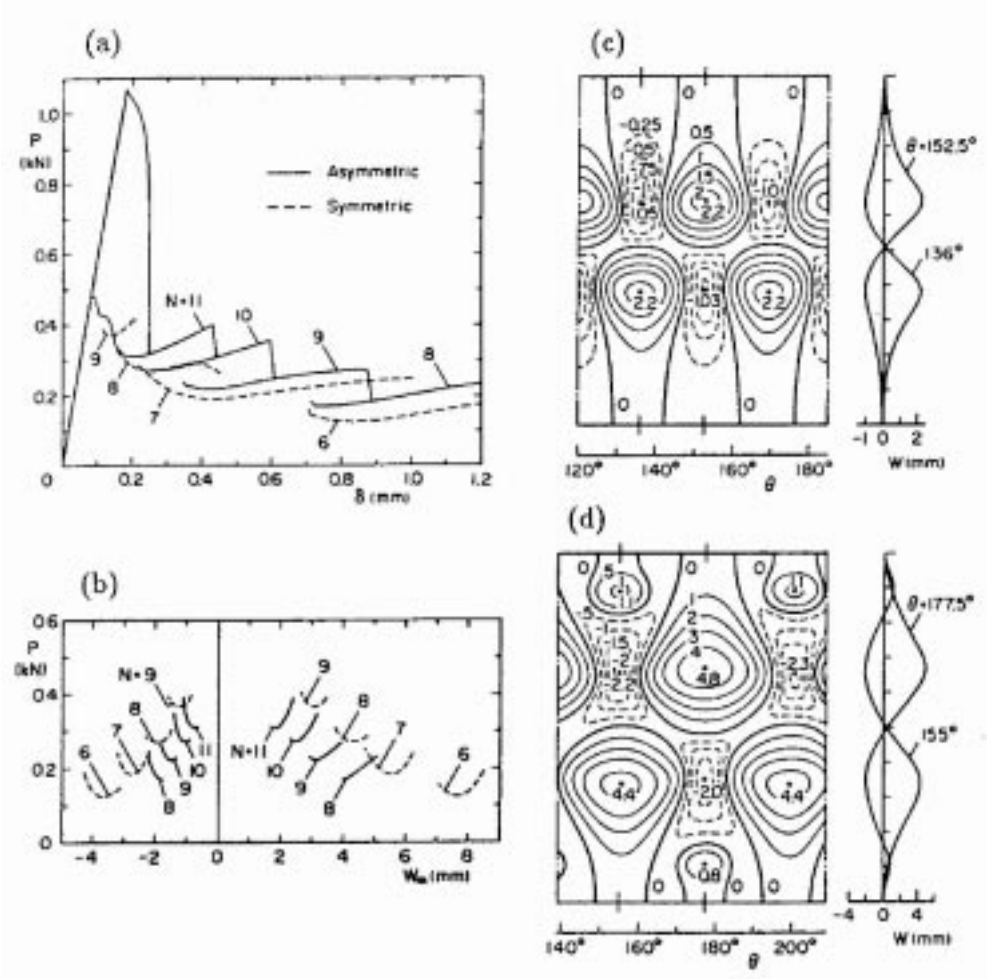

FIGURE 3. Buckling of an elastic cylinder with $L = 160.9$ mm, $R = 100$ mm, $t = 0.247$ mm, $E = 5.56$ GPa, and $\nu = 0.3$ (after Yamaki [19], p.231). (a) load/end-shortening response. (b) load vs. maximum and minimum deflection. (c) buckle pattern for $n = 11$. (d) buckle pattern for $n = 8$.

for the longest cylinder, which goes against the general trend and is likely to have buckled into 3 or more tiers.

3.2. **Dynamical time-stepping finite element analysis.** The same trends can be observed in recent numerical experiments employing dynamical time-stepping routines such as LS-DYNA (see for example [15]). Such simulations avoid some of the pitfalls of purely static formuations, which can be prone to tracking unstable

TABLE 1. Yamaki cylinders: $t = 0.247$ mm, $R = 100$ mm.

L (mm)	Mode	n (expt)	M	n (eq.(2))
22.7	S	18	1	17.7
35.9	S	15	1	15.6
51.0	S	14	1	13.7
71.9	S	12	1	11.9
71.9	A	14	2	15.6
113.9	S	11	1	9.7
113.9	A	12	2	13.1
160.9	S	9	1	8.2
160.9	A	11	2	11.3

TABLE 2. Eßlinger cylinders: $t = 0.254$ mm, $R = 100$ mm

L (mm)	Mode	n (expt)	M	n (eq.(2))
50	S	14	1	13.7
75	S	12	1	11.6
100	A	13	2	13.7
145	A	11	2	11.7
150	A	11	2	11.6
200	A	10	2	10.2
235	A	9	2	9.4
240	A	9	2	9.4
245	A	9	2	9.3
300	A	8	2	8.4
350	A	10	2	7.8
350		10	3	9.5

or barely stable solutions, and when adjusted to model the effects of small imperfections have been found to reproduce accurately the observed behaviour. Schweizerhof *et al* [15] are primarily interested in rapidly-loaded shells, where buckling loads are above those of slow-loading and consequently initial wavelengths are significantly different from those on the Koiter circle. However, they do provide the slowly-loaded case seen here in Fig.4 as a benchmark example.

The buckling sequence is illustrated at a constant end-shortening, as load drops to the stable post-buckling limit with the diamond-pattern asymmetric form shown in the final plot. The dynamical routine self-selects a circumferential wavenumber of $n = 15$. The prediction of (2) gives $n = 15.2$ for $M = 2$, relating to the asymmetric (A) post-buckling mode. The sequence shows a buckling process that involves the growth of a single post-buckling dimple, which stabilizes to the specific determined by $n = 15$ and then propagates circumferentially.

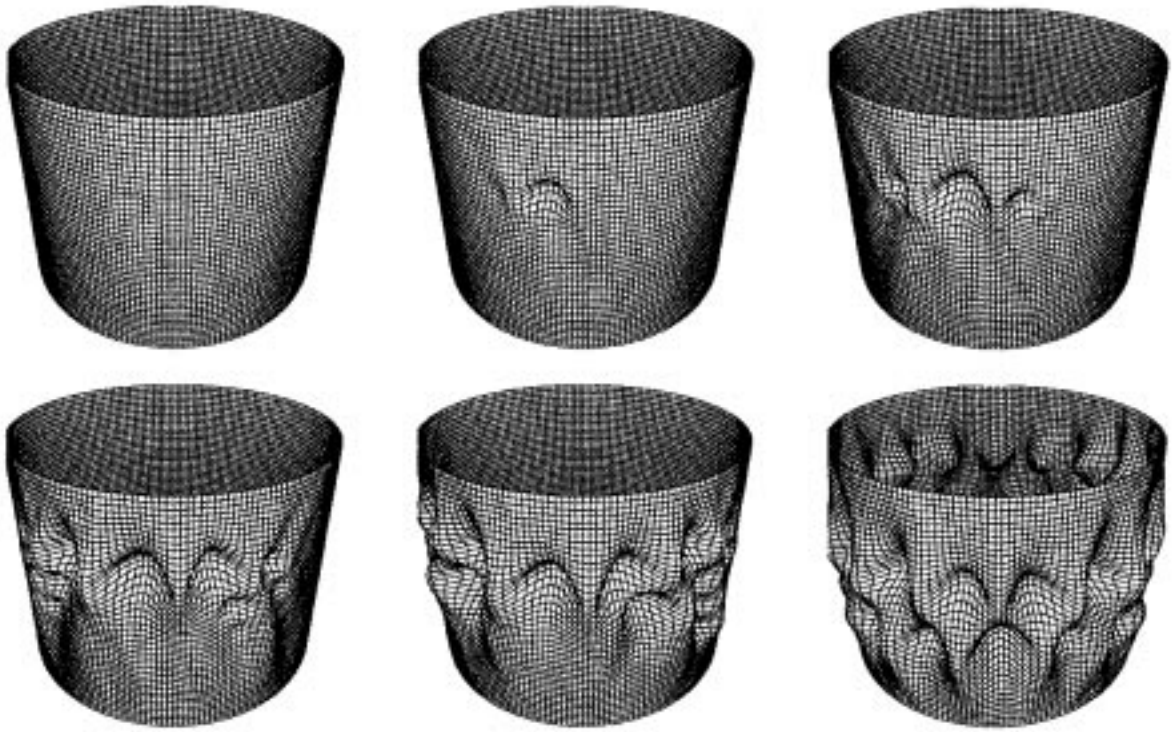

FIGURE 4. Finite element modelling of an imperfect cylinder ($L =$ 966 mm, $R = 625$ mm, $t = 0.56$ mm) using implicit time-stepping procedures (see Schweizerhof *et al* [15]). Growing post-buckling deflections under constrained end-shortening.

4. **Galerkin reduction of von Kármán–Donnell equations.** Post-buckling deflections of a thin (shallow) cylindrical shell of radius R and thickness t can be described by the governing nonlinear von Kármán–Donnell differential equations:

$$\kappa^2\nabla^4 w + \lambda w_{xx} - \rho\phi_{xx} = w_{xx}\phi_{yy} + w_{yy}\phi_{xx} - 2w_{xy}\phi_{xy} \quad (3)$$

$$\nabla^4\phi + \rho w_{xx} = (w_{xy})^2 - w_{xx}w_{yy}, \quad (4)$$

where ∇^4 is the two dimensional bi–harmonic operator, $x \in \mathbb{R}$ is the axial and $y \in [0, 2\pi R)$ is the circumferential co-ordinate, w is the radial displacement measured from a non-trivial (fundamental) unbuckled state, ϕ is a stress function, $\rho = 1/R$, the geometric constant, $\kappa^2 = t^2/12(1-\nu^2)$, ν is Poisson's ratio, the bifurcation parameter, $\lambda = P/Et$, where P is the compressive axial load applied per unit length and E is Young's modulus. Equation (3) is an equilibrium, and equation (4) is a compatibility, equation.

A Galerkin approximation is introduced via the circumferential expansion

$$\begin{aligned} w(x,y) &= \sum_{k=0}^{K-1} a_k(x)\cos(kn\rho y) \\ \phi(x,y) &= \sum_{k=0}^{K-1} b_k(x)\cos(kn\rho y) \qquad n \in \mathbb{N} \end{aligned}$$

for some finite K, where $\cos(n\rho y)$ is referred to as the *seed mode*. The outcome is a system of $8K$ first-order ordinary differential equations in x, that is then solved numerically on a truncated domain under parametric variation of the loading parameter λ, using the continuation code AUTO [6], with boundary conditions which match the symmetry properties at one end (the centre of the localization) and homoclinic (decaying) conditions at the other. This process is described in detail in Lord *et al* [13].

Generally $K = 6$ is found to provide a good compromise between accuracy and numerical efficiency, and a full set of curves for integer values of n running from 8 to 12 is given in Fig.5, on a plot of λ against a measure of the end-shortening,

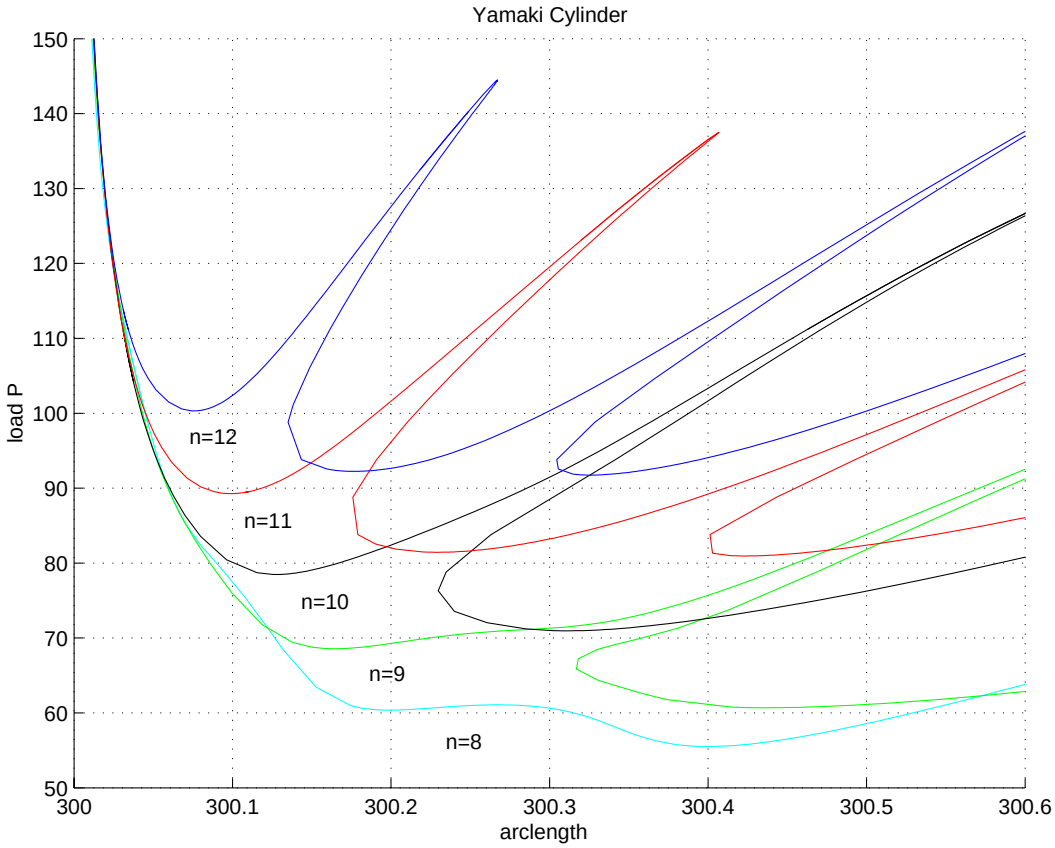

FIGURE 5. Numerically obtained equilibrium paths for cross-symmetric (A) buckling of the longest cylinder of Yamaki [19]: effect of altering the circumferential wavenumber n.

defined by

$$\text{arclength} = \int_0^{\frac{L}{2}} \left[1 + \left(\sum_{k=0}^{K-1} \frac{\partial a_k}{\partial x} \right)^2 \right]^{1/2} \mathrm{d}x, \text{ at } y = 0. \tag{5}$$

All paths are virtually coincident as they emerge from the critical point, but eventually each circumferential wavenumber n results a different snaking form of equilibrium path, as described more fully in Hunt *et al* [10] and illustrated for the particular case of $n = 11$ in Figs.6 and 7. The full picture for a particular n is one

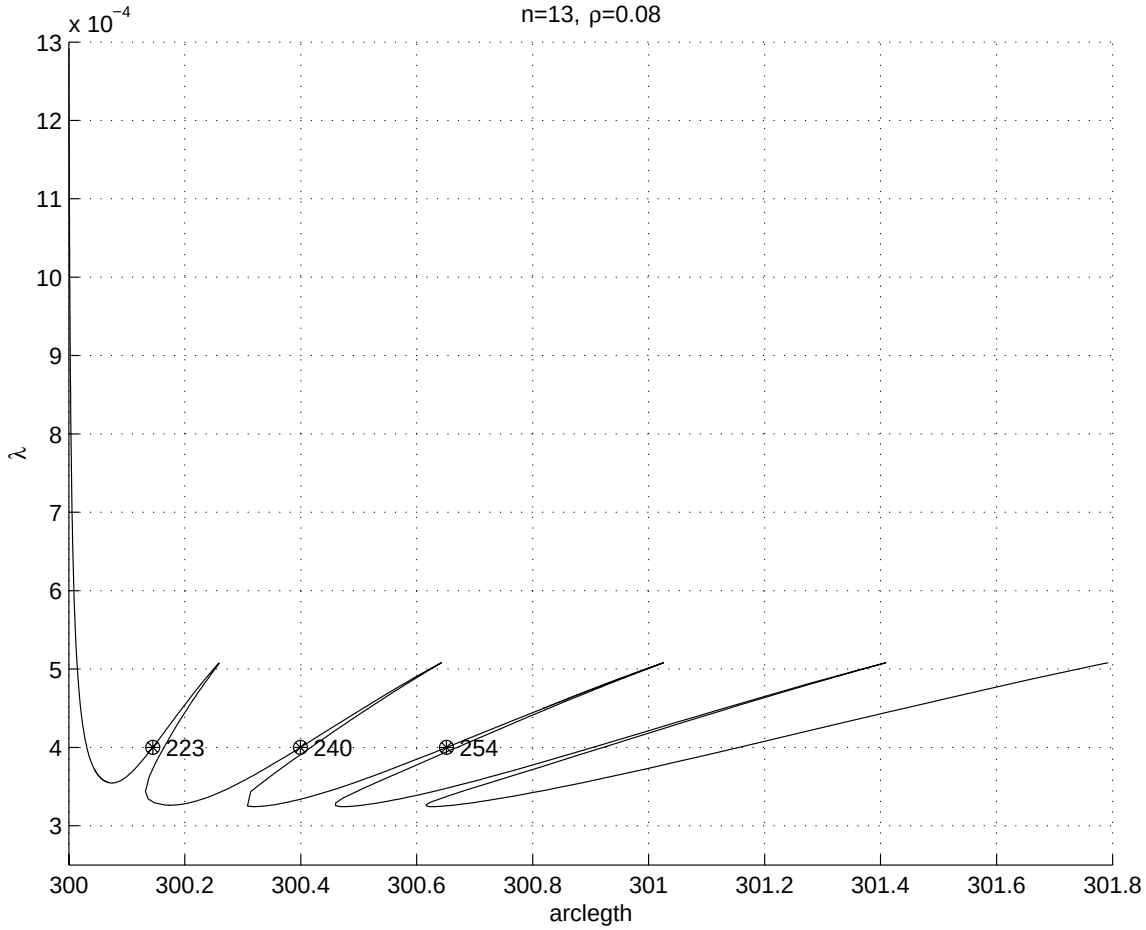

FIGURE 6. Snaking sequence of post-buckling equilibria for a cylinder of dimensions $t = 0.247$, $R = 125$, and for which $n = 13$. Under controlled end-displacement this gives a punctuated or "cellular" form of buckling, in which individual cells buckle in sequential fashion to give the patterns of Fig.7 (see Lord *et al* [13]).

of successive destabilization and restabilization, in a so-called "cellular" buckling sequence. The rapid onset of localization along a typical falling path is clearly seen in Fig.8, where it is found to be effectively complete at load levels commensurate

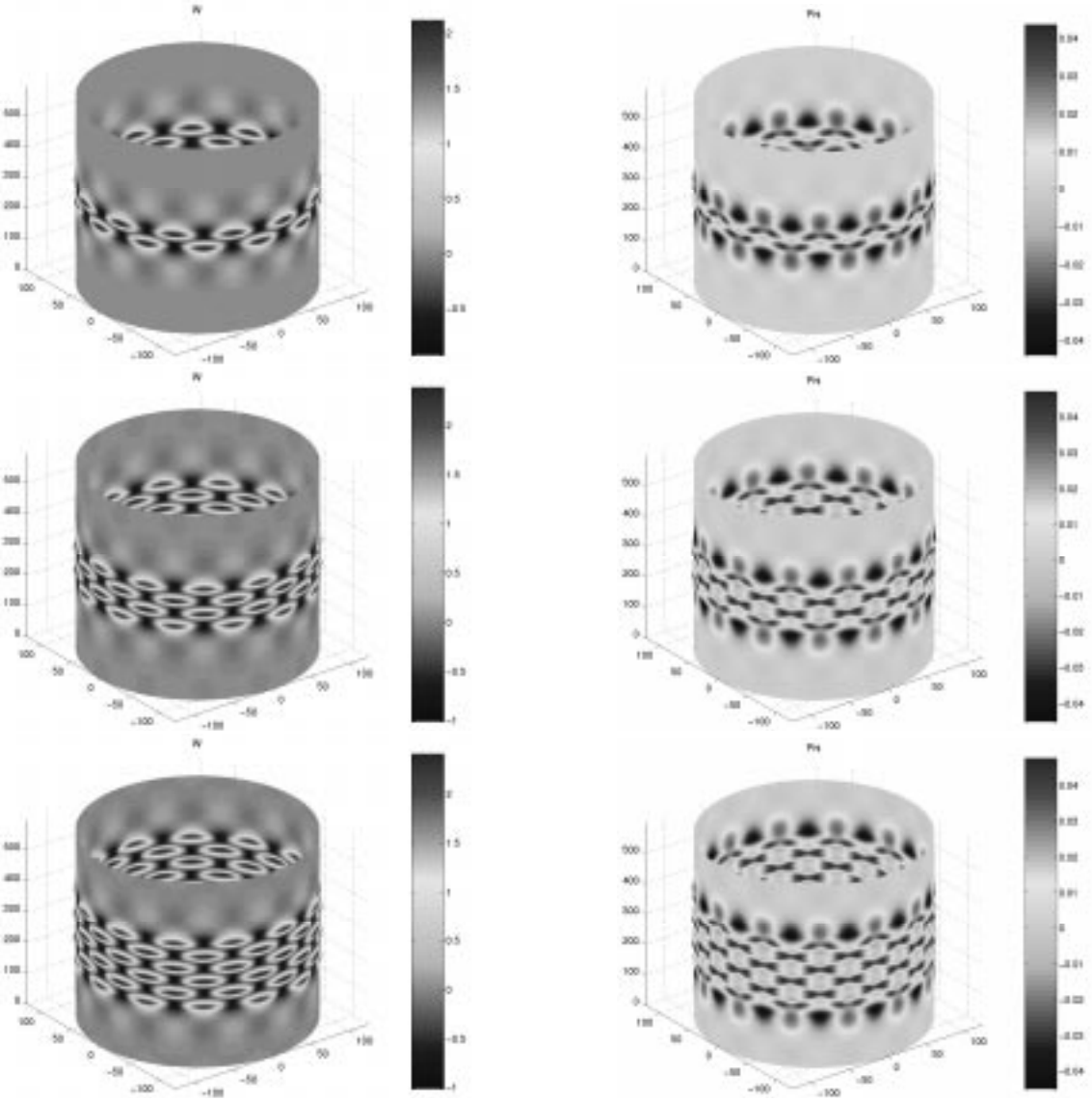

FIGURE 7. Deflection w and stress function ϕ on the snaking path of Fig.6, demonstrating the cellular nature of the buckle pattern. Top, point 223; centre, point 240; bottom, point 254.

with experimental buckling loads. Without some other criterion for selection, it is impossible to determine from the tangle of equilibria shown in Fig.5, the initial expected value of n.

The hypothesis of Section 2 offers just such a criterion, and we next examine both the experimental and the numerical data from a scaling perspective to assess its significance.

5. **Scaling considerations.**

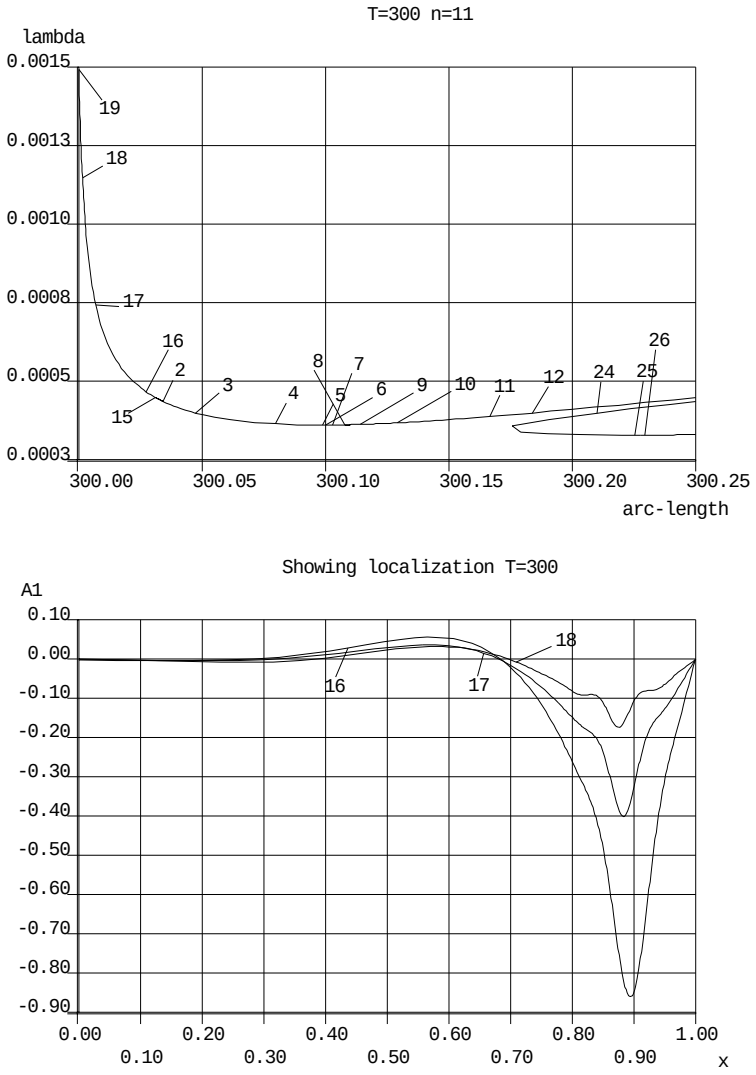

FIGURE 8. (a) Points on initial unloading path for the cylinder of Fig.5 and $n = 11$: (18) $\sigma \approx 0.78\sigma_{\rm crit}$; (17) $\sigma \approx 0.52\sigma_{\rm crit}$; (16) $\sigma \approx 0.30\sigma_{\rm crit}$. (b) Amplitudes of the "seed" Galerkin component a_1 at these points, plotted over the half-length $L/2$.

5.1. **Physical experiments.** As Calladine [5] indicates, the linear eigenvalue result of equation (1), which suggests that the buckling load for cylindrical shells should vary as (t/R), does not square with experimental evidence. Von Kármán, Dunn & Tsien [16] suggest that, for axially-compressed cylinders for which $L/R > 1.5$, experiments scale more as $(t/R)^{1.4}$, whereas Calladine offers a heuristic argument for an exponent of 1.5. To arrive at more objective estimates of such exponents we shall revert to original data, where it occurs in tabular rather than graphical form.

Table 3 describes five different data sets from four teams of experimentalists; for each of these data sets a power law relationship

$$\frac{\sigma_{\rm exp}}{\sigma_{\rm crit}} = a \left(\frac{t}{R} \right)^b \tag{6}$$

has been fit (by the least-squares method). Here $\sigma_{\rm exp}$ is the experimental buckling stress, and it should be noted that $\sigma_{\rm crit}$ of equation (1) itself scales as (t/R).

Reference	R/t range	number of points	a	b
Bridget *et al.* [3]	237–919	15	2.35	0.31
Ballerstedt & Wagner [2]	455–4167	18	3.20	0.32
Donnell (steel) [7]	332–1424	19	2.53	0.36
Donnell (brass) [7]	161–1468	21	1.61	0.30
Lundquist [14]	360–1400	45	10.64	0.49

TABLE 3. Experimental fit to equation (6).

5.2. **Numerical experiments.** Having been computed for the perfect shell, the equilibrium paths of Fig.5 all emerge from the Koiter critical load (1). However, each has a distinctive first minimum, where the response restabilizes. A good approximation to the load level of this first minimum is found in the so-called *Maxwell load*, where the total potential energy of the pre-buckled and post-buckled (periodic) states are the same [11, 10]. If the Maxwell load, rather than the Koiter load, governs the load level of initial buckling, then this might be expected to show up in the scaling with respect to t/R.

Of course, this can only be checked if the relevant circumferential wavelength is known. Fig.9 uses the hypothesis of equation (2) to define this wavenumber, and tracks the first post-buckling minimum for two different L/R ratios as the thickness t is altered, using the continuation code AUTO [6]. These log-log plots appear as straight lines with an index of -1.287 for $R = 100$ and -1.297 for $R = 125$, indicating that the Maxwell load level of our prediction varies approximately as $(t/R)^{1.3}$. This compares well with the experimental evidence reviewed in the previous section, and is significantly different from the linear scaling suggested by the Koiter load expression (1).

6. **Concluding Remarks.** In an attempt to untangle the plethora of equilibrium paths seen in Fig.5, we suggest here that the circumferential wavenumber n can be picked from the small-deflection Koiter circle load (1). This relies on two separate conjectures – that a long ($M = 1$ or 2) wavelength mode, from amongst all other possibilities, acts as the triggering instability, and that the circumferential wavenumber thus produced persists far into the post-buckling range. We can offer no proof for either of these suppositions. Instead, we have reviewed a mix of experimental and numerical evidence from two complementary angles. First, there are direct experimental wavecounts, seen for example in the two sets of tabulated data from [19] and [8]. Secondly, there is the evidence of the numerical scaling law employing the prediction, which reflects the scaling found by a number of different experimentalists.

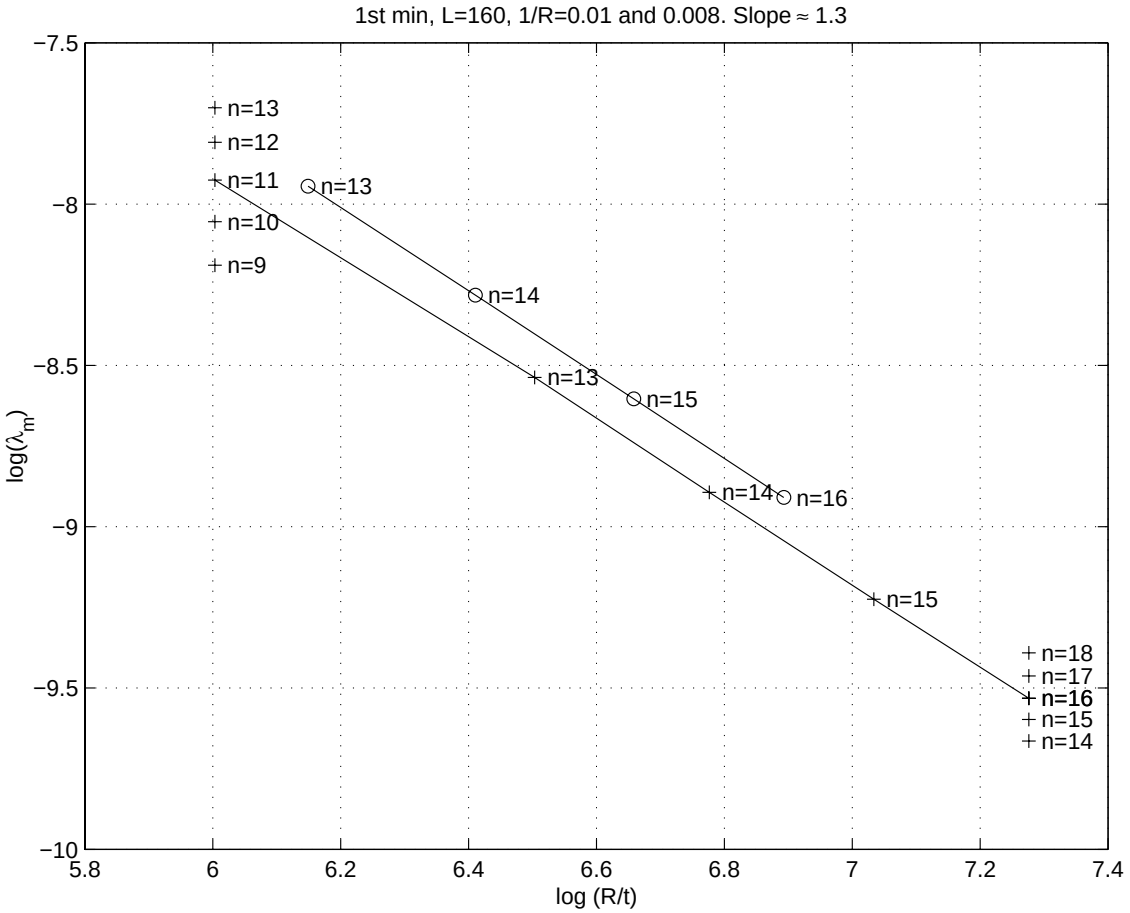

FIGURE 9. Scaling law from numerical experiments. Lower line, $R = 100$; upper line, $R = 125$. Crosses at $\log(R/t) = 6.0$ denote the minima of Fig.5.

The first conjecture, that long waves are picked from the Koiter circle to the exclusion of others, was suggested by Yamada & Croll [18] for short cylinders buckling into the symmetric (S) mode, and we explore it no further here. The second, that the periodic wavenumber as seen in the pre-buckling state persists into advanced post-buckling, is worthy of futher discussion. Long structures with stable (plate-like) post-buckling responses and periodic or near-periodic buckling modes are known to exhibit mode-locking and mode-jumping phenomena [9]. The present periodicity, although orthogonal to the direction of loading and part of an unstable buckling process, is nevertheless prone to the same mechanisms. An imposed periodicity can be maintained, or a jump can take place to a different periodic state, but unlike for localized responses, smooth transition is ruled out. It is therefore not altogether surprising that the circumferential peridocitiy is retained, although attempts to define axial wavelengths in the post-buckling range are likely to be unsuccessful.

It is interesting in this regard to compare and contrast the pre-buckled shape seen experimentally by Arbocz & Babcock [1] (middle plot, Fig.2), with the post-buckling shape seen on the falling post-buckling path in the numerical simulations (point 18, Fig.8). Both appear at about the same relative load level, and therefore would appear close to one another on a load/end-shortening plot. However, the experimental point is stable (just before buckling), while the latter is unstable and would not be seen in a normal loading sequence. It therefore represents an energy hump, which the shell must surmount before ultimately reaching the stable post-minimum state. This hump is clearly easily eroded by imperfections, and a significant numerical challenge is therefore to be found in the search for an algorithm to describe a route to instability that might mirror this. Numerical [15] and experimental [8] evidence suggests that such a route may be through the growth of a single dimple on the shell surface. As such equilibrium states are unstable, this is likely to require some kind of "mountain pass" algorithm.

REFERENCES

[1] J. Arbocz and C. D. Babcock. The effect of general imperfections on the buckling of cylindrical shells. *ASME J. Appl. Mech.*, 36:28–38, 1969.

[2] W. Ballerstedt and H. Wagner. Versuche über die Festigkeit dünner unversteifter Zylinderunter Schub- und Längskräften. *Luftfahrtforschung*, 13:309–312, 1936.

[3] F. J. Bridget, C. C Jerome, and A. B. Vosseller. Some new experiments on buckling of thin-wall construction. *Trans. ASME Aero. Eng.*, 56:569–578, 1934.

[4] C. J. Budd, G. W. Hunt, and R. Kuske. Asymptotics of cellular buckling close to the Maxwell load. *Proc. R. Soc. Lond.*, A 457:2935–2964, 2001.

[5] C. R. Calladine. A shell-buckling paradox resolved. In D. Durban, G. Givoli, and J. G. Simmonds, editors, *Advances in the Mechanics of Plates and Shells*, pages 119–134. Kluwer Academic Publishers, Dordrecht, 2000.

[6] E.J Doedel, A.R Champneys, T.R. Fairgrieve, Yu.A. Kuznetsov, B. Sandstede, and X.J. Wang. AUTO97 continuation and bifurcation software for ordinary differential equations, 1997. Available by anonymous ftp from FTP.CS.CONCORDIA.CA, directory PUB/DOEDEL/AUTO.

[7] L. H. Donnell. A new theory for buckling of thin cylinders under axial compression and bending. *Trans. ASME Aero. Eng.*, AER-56-12:795–806, 1934.

[8] M. Eßlinger and B. Geier. Gerechnete Nachbeullasten als untere Grenze der experimentallen axialen Beullasten von Kreiszylindern. *Der Stahlbau*, 41(12):353–359, 1972.

[9] P. R. Everall and G. W. Hunt. Mode jumping in the buckling of struts and plates: a comparative study. *Int. J. Non-Linear Mech.*, 35:1067–1079, 2000.

[10] G. W. Hunt, G. J. Lord, and A. R. Champneys. Homoclinic and heteroclinic orbits underlying the post-buckling of axially-compressed cylindrical shells. *Comput. Methods Appl. Mech. Engng.*, 170:239–251, 1999.

[11] G. W. Hunt and E. Lucena Neto. Maxwell critical loads for axially loaded cylindrical shells. *ASME J. Appl. Mech.*, 60(3):702–706, 1993.

[12] W. T. Koiter. *On the stability of elastic equilibrium.* PhD thesis, Technische Hogeschool, Delft (Technological University of Delft), Holland, 1945. English translation issued as NASA, *Tech. Trans.,* **F 10**, 833, 1967.

[13] G. J. Lord, A. R. Champneys, and G. W. Hunt. Computation of homoclinic orbits in partial differential equations: an application to cylindrical shell buckling. *SIAM J. Sci. Comp.*, 21(2):591–619, 1999.

[14] E. Lundquist. Strength tests of thin-walled duralumin cylinders in compression. Technical report, 1933. NACA Rept 473.

[15] K. Schweizerhof, R. Hauptmann, T. Rottner, and M. Raabe. Silo buckling analyses considering nonuniform filling – dynamic versus static analyses using LS-DYNA. Proc. 5th Int. LS-DYNA Conf., Southfield, Michigan, 1998.

[16] T. von Kármán, L. G. Dunn, and H. S. Tsien. The influence of curvature on the buckling characteristics of structures. *J. Aero. Sciences*, 7:276–289, 1940.

[17] M. Khurram Wadee. The elastic strut on elastic foundation: a model localized buckling problem. In A. R. Champneys, G. W. Hunt, and J. M. T. Thompson, editors, *Localization and solitary waves in solid mechanics*, pages 31–53. World Scientific Publishing, Singapore, 1999.

[18] S. Yamada and J. G. A. Croll. Contributions to understanding the behavior of axially compressed cylinders. *ASME J. Appl. Mech.*, 66:299–309, 1999.

[19] N. Yamaki. *Elastic Stability of Circular Cylindrical Shells*, volume 27 of *Applied Mathematics and Mechanics*. Elsevier, 1984.